CONSEIL INTERNATIONAL DES MACHINES A COMBUSTION

INTERNATIONAL COUNCIL ON COMBUSTION ENGINES

A PREDICITIVE MODEL FOR CATALYTIC CONVERTERS ON STATIONARY INTERNAL-COMBUSTION ENGINES
PAPER NO.: 226

Joe Aleixo, Ming Chen, Thierry Leprince, Shazam Williams

DCL International Inc.

SUMMARY

This paper describes the details of a predictive model specifically designed for catalytic converters used for stationary industrial engines. This model uses inputs such as engine emission characteristics, fuel, exhaust system design and engine duty cycle.

The architecture of the model provides two main modes of computation: transient conditions and steady state conditions. The shared items and simplifying assumptions for deriving a steady state solution from a generalized transient model is discussed. The applications and limitations of both modes of calculation are discussed.

Correlations for reaction kinetics are based on pseudo-first order reaction rates with pore diffusion resistance and an Arrhenius expression for the reaction rate coefficient. Correlations for mass transfer are based on the boundary layer model. Details on the development of these correlations are provided. Information is also provided on the correlating of the physical properties of substrates to pressure drop and conversion efficiency.

The model is flexible for many catalytic converter types, such as three-way, oxidation and selective catalytic reduction. The model is also flexible for different cell densities, cell shapes and substrate types such as metal and ceramic.

The influence of fuel composition on engine out hydrocarbon emissions is briefly discussed with respect to natural gas fuelled engines. It is shown that it is necessary to take into account the fuel composition of natural gas when predicting conversion efficiency of hydrocarbons on catalytic converters used with lean-burn natural gas fuelled engines.

A method for quantifying deterioration rates for catalysts for long-term operation is also described. This method assumes that catalyst deterioration can be grouped into two mechanisms: the first involving deterioration of the catalyst activity in terms of changes to the reaction rate coefficient, and the second involving deterioration or masking of the substrate by applying a deterioration term to the mass transfer coefficient.

The validity of the model is shown by example case studies, where results show excellent correlation between the model and test cell and field data for a wide range of engines, catalyst types and operating conditions.

CONCLUSIONS

The validity of the model is demonstrated by example case studies, where results show excellent correlation between the model and test cell and field data for a wide range of engines, catalyst types and operating conditions. A general mass transfer correlation for three-way, oxidation and SCR catalysts is demonstrated to be applicable for a variety of pollutant species, catalyst geometries, and cell densities.

INTRODUCTION

The catalytic converter is employed in a wide variety of industrial engines, including engines used for power generation, co-generation, gas compression and other stationary and industrial applications. In recent years advances have been made in computer modelling of catalytic converters to assist in design optimization, with most of this work focused toward the automotive industry [1-4]. The set-up requirements for these simulations can be time consuming and the solutions computationally intensive.

The purpose of this paper is to adapt these modelling concepts to stationary and industrial engine applications. Due to emission regulations, the engine out emission requirements for many stationary applications are often determined on a site-specific basis. Therefore it is necessary to have a model that can provide relatively quick results on number of design variations without compromising accuracy. This model applies to natural gas, LPG and diesel fuels, and for three-way, selective catalytic reduction and oxidation catalyst types.

A list of the reactions considered in the model is provided in Table 1.

Figure 1 provides a physical concept of the catalytic converter and the processes taking place. The channel walls contain a porous high surface area material or washcoat with catalytically active sites. Catalytic reactions take place on these active sites. The seven general steps involved in catalytic reactions are described in Figure 2, and include mass transfer between the bulk gas and washcoat surface, pore diffusion, adsorption/desorption and intrinsic reaction.

Figure 2 – Reaction Steps on Monolith Catalyst (Exaggerated scale)

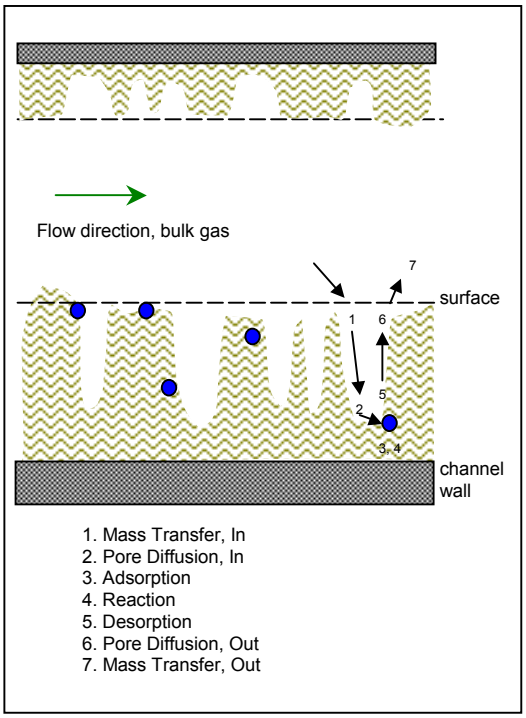

Figure 1 – Catalytic Converter for Industrial Engine

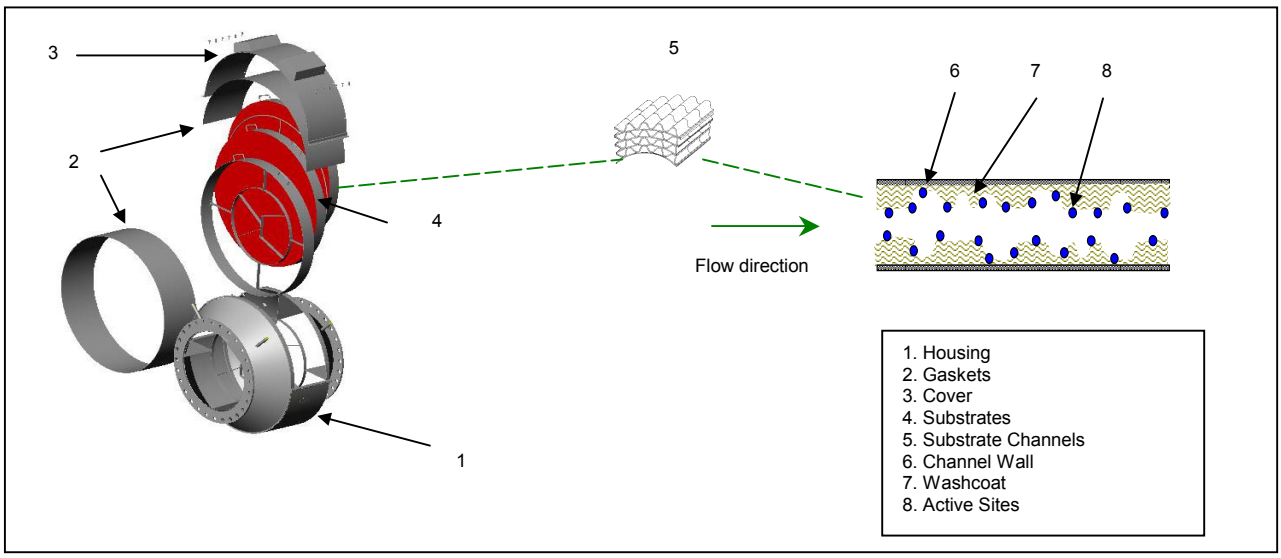

Table 1 – Model reaction list

Oxidation	$CO + ½ O_2 \rightarrow CO_2$ $CH_4 + 2 O_2 \rightarrow CO_2 + 2 H_2O$ $CH_2O + O_2 \rightarrow CO_2 + H_2O$ $C_2H_4 + 3 O_2 \rightarrow 2 CO_2 + 2 H_2O$ $C_2H_6 + 3.5 O_2 \rightarrow 2 CO_2 + 3 H_2O$ $C_3H_6 + 4.5 O_2 \rightarrow 3 CO_2 + 3 H_2O$ $C_3H_8 + 5 O_2 \rightarrow 3 CO_2 + 4 H_2O$ $n\text{-}C_4H_{10} + 6.5 O_2 \rightarrow 4 CO_2 + 5 H_2O$ $n\text{-}C_8H_{20} + 13 O_2 \rightarrow 8 CO_2 + 10 H_2O$
Three-Way	$CO + NO \rightarrow CO_2 + ½ N_2$
SCR	$4 NO + 4 NH_3 + O_2 \rightarrow 4 N_2 + 6 H_2O$

MODEL OVERVIEW

The core of the model contains two computational routines: one for steady state mode and one for transient mode. The steady state mode is suitable for catalyst selection for most stationary engines and allows rapid computation of catalyst performance for engines operating at a steady load and speed. The steady state mode may also be used for determining weighted emissions where a duty cycle involves a series of steady state modes, such as the ISO 8178 test cycles.

The transient mode allows computation of catalyst performance where the engine operating characteristics such as exhaust temperature, exhaust flow and emissions levels are time dependent.

The following groups of data were developed and incorporated into the model:

1. Experimental and field data on catalyst conversion efficiencies for a variety of test conditions (over 400 operating conditions).
2. Coefficients related to mass transfer, heat transfer and reaction kinetics.
3. Physical and chemical deterioration factors (DF) for substrates and catalytic coatings under normal operating conditions.
4. Physical properties for substrates, including geometric surface area, channel diameter and wall thickness.
5. Look up tables for flow distribution, based on flow velocity, Reynolds number and pipe and substrate geometry.

The computational routines of the catalyst model are based on the following assumptions:

- One dimensional “plug flow” or “tubular reactor” model.
- Axial diffusion of mass and heat in the gas phase is neglected.
- First and second order reaction rates (one step reaction).
- No interactions among pollutants.
- Adiabatic conditions for the catalytic converter.

Computations are expanded into 2-D, by coupling the 1-D model to a look-up table of flow distributions for various geometries and flow conditions, obtained in Fluent™ CFD.

As a simplifying assumption, surface reactions were not explicitly modeled, i.e. no surface reaction and no adsorption/desorption mechanisms were used. Instead surface reactions were bulked into a pseudo-first order reaction kinetic term for each species with an effectiveness factor term to quantify the pore diffusion effects.

The mass transfer coefficients and statistical confidence levels for these coefficients were created from the experimental results data and could be updated and refined as more data is entered.

A summary of the input data required for catalyst sizing is provided in Table 2. A screenshot of the application engineering user interface is provided in Figure 3.

Figure 3 – Input Screen

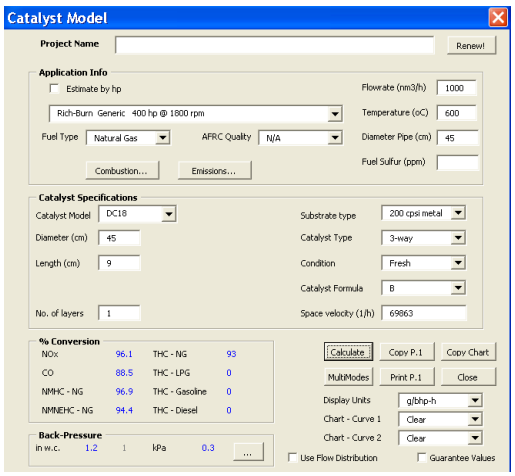

Table 2 – Inputs List

Engine	- Exhaust flowrate - Exhaust temperature - Inlet pipe diameter - Engine-out emissions levels - AFRC quality (for three-way catalyst only) - Fuel type
Catalyst	- Catalyst dimensions - Substrate physical characteristics - Catalyst formula - Catalyst age (operating hours)

STEADY STATE EXPRESSIONS

The general solution for the steady state model is based on the one dimensional “plugflow“ or “tubular reactor” model. The mass balance equation on a single control volume is given as

(Molar rate in) - (molar rate out) + (molar rate reacted) = 0

or,

$$F_{in} - F_{out} + raA_c\Delta z = 0 \qquad (1)$$

Since the catalytic reactions take place on active sites, in order for a molecule to react it must first travel from the bulk gas to the surface of the catalytic site, according to the steps described in Figure 2. If we bulk all these steps into one overall rate step and assume a first order reaction rate, $r = -K_{overall}C_{As}$, then equation 1 can be re-arranged into the derivative form and solved to give the following solution [5],

$$X = 1 - e^{K_{overall}a(L/v)} \qquad (2)$$

Although many of the reaction rates encountered are not true first order reactions, in many cases, pseudo first order reactions can be used to yield acceptable results with minimum complexity to the computation.

If we assume a film model to describe the mass transfer of species from the bulk gas to the catalyst surface (step 1 in Figure 2), assume steps 2 to 6 can be bulked into one overall rate step, assume step 7 is not a rate-limiting step, and assume no accumulation or loss, then the rate of reaction of species A is the same as the flux of species A to the surface of the catalyst, giving

$$k_c(C_A - C_{As}) = k_r C_{As} \qquad (3)$$

Where k_c is the mass transfer term coefficient (step 1), and k_r is the kinetic rate term (describing steps 2 to 6). Rearranging equation (3) yields [5]

$$\frac{1}{K_{overall}} = \frac{1}{k_r} + \frac{1}{k_c} \qquad (4)$$

The reaction rate term k_r includes the effects of pore diffusion resistance, the amount of catalyst sites, washcoat properties and the intrinsic reaction adsorption/desorption and reaction rate. It is assumed that for oxidation reactions, the term is zero order dependent on oxygen and therefore oxygen concentration becomes implicit to the intrinsic reaction rate term. The term k_r is therefore expanded as follows

$$k_r = \eta c_{pgm}^{\gamma} \rho_{wc} S_{BET} k_r^i \qquad (5)$$

Although the washcoat is a relatively thin coating on the substrate, under certain conditions the catalytically active sites on the bottom of the layer may not be as effectively utilized as those in the top of the washcoat layer. The washcoat layer is permeable to molecular diffusion, but provides resistance. The effectiveness factor (η) given in Equation (5) is a dimensionless number added to the reaction rate term in order to account for pore diffusion resistance of the washcoat. The magnitude of the effectiveness factor (ranging from 0 to 1) indicates the relative importance of pore diffusion resistance. A method for determining the effectiveness factor is provided in [6]. A calculation

showing satisfactory results for an automotive catalyst is provide in [4].

The Arrhenius expression is used to describe the intrinsic reaction rate term.

$$k_r^i = Ae^{-\frac{E_A}{RT}} \qquad (6)$$

Pseudo-first order reaction rates are used for the reactions, with activation energy (E_A) and frequency factor (A) determined experimentally. A discussion on determining terms for reaction rate is provided in [7].

More detailed expressions such as Langmuir-Hinshelwood are available in the literature, incorporatingnon-first order reaction rate terms and inhibition terms. Under these conditions $K_{overall}$ is dependent on the species concentrations. An approximate solution using Equation 2 is obtained if the substrate is divided into a series of longitudinal elements and $K_{overall}$ is recalculated for each element using an iterative method. The additional detail of these expressions is not considered in this paper, since they become important only under low temperature operation such as cold start behaviour, which is generally not pertinent in the duty cycles for stationary engines.

Since the mass transfer coefficient k_c is dependent on the amount of specific geometric surface area on the catalyst monolith, we can write,

$$k_c = k_c^i a \qquad (7)$$

The overall rate constant can then take the following form:

$$\frac{1}{K_{overall}} = \frac{1}{\eta c_{pgm}^{\gamma} \rho_{wc} S_{BET} k_r^i} + \frac{1}{k_c^i a} \qquad (8)$$

In practice for most catalyst applications, two limiting cases arise. Under high temperature conditions the concentration gradient exists as shown in Figure 4, indicating the reaction is controlled by the flux of molecules from the bulk gas to the surface of the catalyst, as shown in case (a). The rate of mass transfer from the bulk gas to the catalyst surface is determined by the mass transfer coefficient, k_c. This coefficient is mainly dependent on the Reynolds number and geometry of the channel inside the substrate. Under these conditions, k_r is much larger than k_c resulting in $K_{overall} \approx k_c$, that is, conversion efficiency is determined by the amount of geometric surface area of the catalyst substrate. Under low temperature conditions a small concentration gradient exists, showing the reaction is controlled by the intrinsic kinetic rate. Under low temperature operation, steps 2 to 6 are important, causing k_r to be very small and $K_{overall} \approx k_r$, that is, conversion efficiency is determined by the intrinsic catalyst kinetics or activity.

TRANSIENT EQUATIONS

The basic equations for the model consist of a mass balance for the gas phase (Equation 9), an energy balance for the gas phase (Equation 10), an energy balance for the solid phase (Equation 11), and a mass balance for the reacting species [8, 9]. If first order reaction rates are assumed, then the explicit equation for mass balance in the solid phase can be eliminated and replaced with an overall reaction rate term ($K_{overall}$) (Equation 12).

$$\varepsilon \frac{\partial C_{g,i}}{\partial t} = -v \frac{\partial C_{g,i}}{\partial z} - K_{overall} a C_{g,i}, \qquad i = 1,2,..,N_{species} \qquad (9)$$

$$\varepsilon \rho_g C_{pg} \frac{\partial T_g}{\partial t} = -v \rho_g C_{pg} \frac{\partial T_g}{\partial z} + h\, a\, (T_s - T_g) \qquad (10)$$

Figure 4 – Pollutant concentration profile

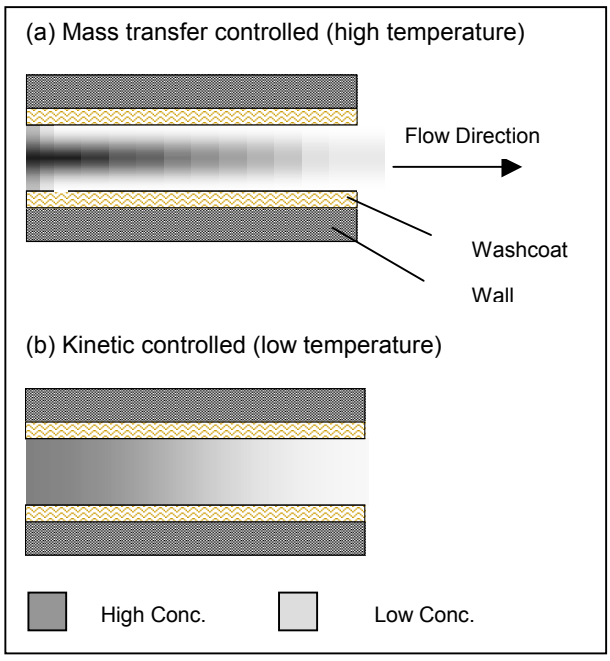

$$(1-\varepsilon)\rho_s C_{ps}\frac{\partial T_s}{\partial t} = \lambda_s(1-\varepsilon)\frac{\partial^2 T_s}{\partial z^2} + h\,a\,(T_g - T_s) + \sum_{i=1}^{N_{species}}(-\Delta H)_i \frac{\dot{m}_g}{\pi R^2 M_g}\frac{\partial C_{g,i}}{\partial z} \quad (11)$$

$$\frac{1}{K_{overall}} = \frac{1}{\eta\, C_{Pt}^{\varpi}\; k_r^i \rho_{wc} S_{BET} C_{o_2}} + \frac{1}{a\, k_c^i} \quad (12)$$

For a given species the overall reaction rate term is determined from the bulked reaction rate taking place at the catalyst surface (the middle term of Equation 12) and the mass transfer rate of species from the bulk gas to the catalyst surface (the right-hand term of Equation 12). With oxygen in excess, the mole fraction of oxygen at the surface can be assumed the same as in the bulk gas. The heat transfer, mass transfer and kinetic rate expressions were developed from model gas reactor and engine test cell data.

To obtain the numerical solution, the length along the catalytic converter is divided into a number of longitude computational elements and the corresponding finite difference relations are approximated. As the first step the gas temperature is solved iteratively until convergence is achieved. Next the reaction rates are solved for each species using a fourth order Runge-Kutta method, and finally solid temperature is solved. This method normally achieves a solution in several minutes using a recent model desktop PC, allowing a number of design variations to be quickly assessed.

MASS TRANSFER

The following correlation was selected to describe mass transfer between the bulk gas and the catalyst surface, based on earlier studies of monolith type catalysts [3,5]:

$$N_{sh} = b_1 (N_{\mathrm{Re}} N_{Sc})^{b_2} \quad (13)$$

where b_1 and b_2 are experimentally determined constants, and modified versions of the Reynolds number, $N_{\mathrm{Re}} = \frac{\rho_g V}{\mu a}$ and Sherwood number, $N_{Sh} = \frac{k_c}{D_{AB} a}$ are used, incorporating the specific geometric surface area of the substrate. Correlation data points are provided in Figure 14.

PRESSURE DROP

Flow through the monolithic substrate channels is laminar. The Hagen-Poiseuille equation is used to calculate pressure drop and standard correlations for substrate entrance and exit effects are applied [10, 11]. Pressure drop due to inlet and outlet cone effects are determined from CFD Fluent™ for a variety of geometry configurations and provided in a look-up table.

FLOW DISTRIBUTION

In order to expand the model from one dimension to two dimensions one needs to predict the flow field in the exhaust pipes, cones and catalyst substrates. For this model, CFD Fluent™ was used to generate a series of flow fields for a variety of operating conditions and catalyst geometry configurations.

The flow field data was organized into a series of look-up tables. The flow in the catalytic converter is determined by the geometrical configuration of the catalytic converter and the inlet pipe, the flow resistance characteristic of the substrate, and the Reynolds number. The appropriate flow field data is chosen from the table based on these characteristics.

Figure 5 show the contours of the static pressure and the velocity vectors at a cross section, respectively. It is shown that a large recirculation zone is formed in the diffuser. When the flow enters the substrate zone, it aligns with the channel direction.

The flow in the substrate is considered fully laminar and is represented by a porous zone. The flow in the rest part of the domain is turbulent. The turbulence is modeled by the standard k-ε turbulence model. The mesh consists of 92900 non-uniform hexahedral cells.

Figure 6 provides a summary of flow uniformity for two dimensional flow at the inlet face of the catalyst in terms of the flow uniformity index [11]. The uniformity decreases with increasing Reynolds number or mean flow velocity. The flow uniformity

also decreases with increasing catalyst diameter to inlet pipe diameter ratio.

Figure 7 provides the calculated axial flow velocity at the inlet face of the substrate for an inlet exhaust temperature of 420 ^{o}C, inlet cone angle of 45 deg., and a substrate to pipe diameter ratio of 3.0.

Figure 5 - The velocity vectors on the cross section. The cell density is 300 cpsi, and the Reynolds number is 16300.

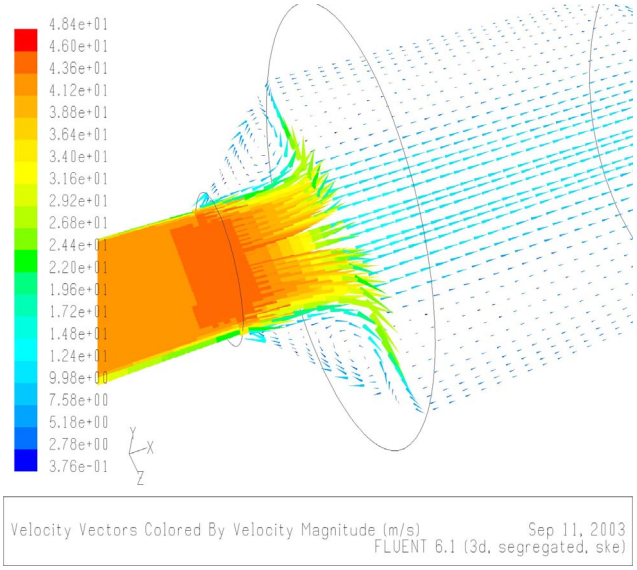

Figure 6 - The calculated flow uniformity index, γ, at the front face of the substrate. Both the Reynolds number and the cell density are varied. The substrate is metallic.

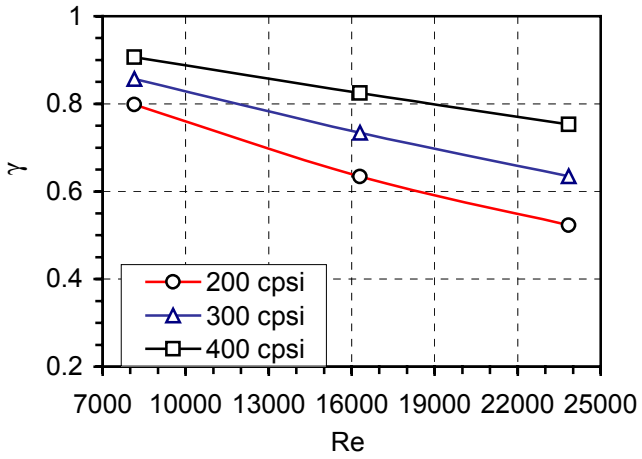

Figure 7 - The calculated profiles of axial flow velocity at the inlet face of the substrate, as a function of non-dimensional radius and metal substrate of cell density of 300 cpsi.

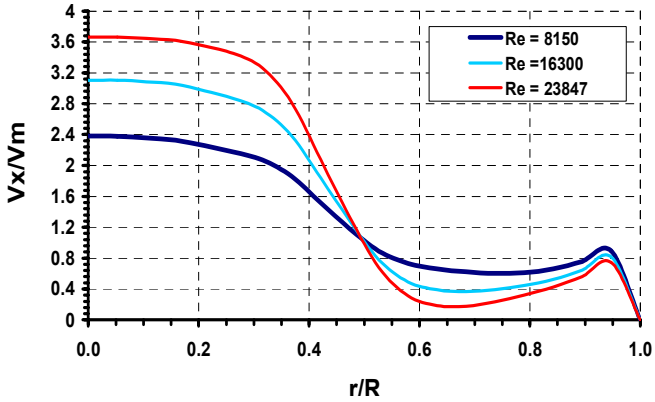

CATALYST DETERIORATION FACTORS

Table 3 provides a detailed list of issues that contribute to catalyst deterioration. Figure 8 provides a typical deterioration factor (DF) chart for CO with operating time. Unfortunately this approach provides only empirical information based on a unique set of circumstances.

An alternate method for quantifying deterioration rates for catalysts for long-term operation is useful if it can be applied more broadly for a wide variety of catalysts and conditions. This method assumes that catalyst deterioration can be grouped into two mechanisms: the first involving deterioration of the catalyst activity in terms of changes to the reaction rate coefficient, and the second involving deterioration or masking of the active surfaces of the substrate by applying a deterioration term to the mass transfer coefficient. The following approach is used for calculation of DF.

1. Mass transfer from the bulk gas to the catalyst surface decreases over time. This is due to erosion of washcoat and physical masking caused by ash deposits.

2. Pore diffusion rates decrease with time as metal and phosphorus deposits on the washcoat, blocking some pores.

3. Catalyst activity decreases with time as poisons deposit on the catalyst sites, and additional active sites are lost due to sintering.

For three-way catalysts a fourth term is assumed, that is the loss of oxygen storage capacity (OSC) due to high temperature conditions. OSC loss, combined with the frequency, amplitude and quality of air-fuel ratio control is lumped into the kinetic rate term by an adjusting parameter.

Figure 8 – Catalyst-out emissions from a three-way catalyst

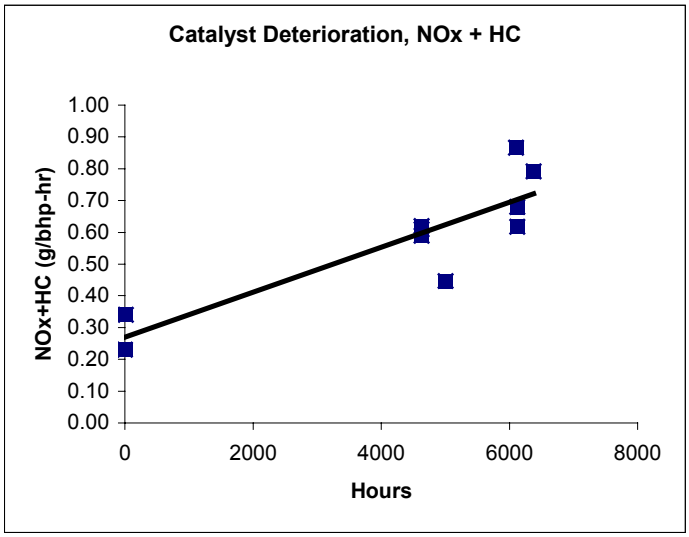

Table 3 – Catalyst Poison Mechanisms [12]

Chemical
- Poisoning; irreversible adsorption or reaction on/with the surface
- Inhibition; competitive reversible adsorption of the poison precursors

Thermal
- Sintering (re-dispersion)
- Alloying
- Support changes
- Noble metal-base metal interactions

Fouling
- Carbonaceous deposits (coking)

Mechanical
- Thermal shock
- Attrition/erosion
- Physical breakage

EXHAUST COMPOSITION

Hydrocarbons or volatile organic compounds (VOCs) in the exhaust are often assumed as unburned fuel, and in some cases one or two representative species are used to describe the hydrocarbon mixture in the exhaust. Unfortunately this is far from the case in lean burn gas fueled engines. It is important to predict the speciation of hydrocarbons for lean-burn natural gas engines because of the wide range of light-off temperatures for the different species. CH_4 is essentially non-reactive at low temperature. Ethane and propane also have relatively high light-off temperatures. Longer chained hydrocarbons, paraffins as well as formaldehyde have relatively low light-off temperatures.

The composition of hydrocarbons in the exhaust is dependent on the engine design characteristics, engine operating conditions, as well as the fuel composition of the natural gas. Due to such variability of the fuel composition, for an accurate prediction of hydrocarbon conversion efficiency one must take into consideration the site-specific fuel composition and the effects of the combustion process on the engine out hydrocarbon emissions.

For natural gas fuel, the relative fraction of formaldehyde is increased in the exhaust gas, as it is an intermediate species in the combustion process [17]. Empirical data on engine out emissions for formaldehyde is provided in Figure 10. Further detail on mechanisms of in-cylinder combustion is outside of the scope of this paper.

A description of the coupling of the hydrocarbon speciation model with the catalyst model is shown in Figure 9. For the engine test described in Table 4, a comparison of hydrocarbon fraction in the fuel to the measured hydrocarbon fraction in the exhaust, and the predicted hydrocarbon fraction in the exhaust using an empirical combustion model is provided in Figure 13.

Figure 9 – Coupling of combustion model with catalyst model for prediction of non-methane hydrocarbon and non-methane non-ethane hydrocarbon conversion

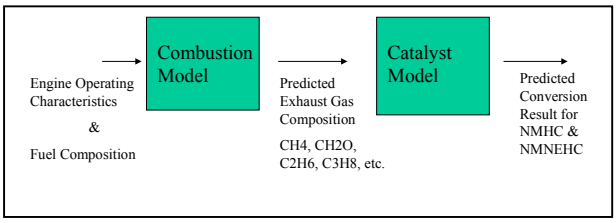

Figure 10 – Formaldehyde in engine exhaust as a fraction of fuel input [13, 14]

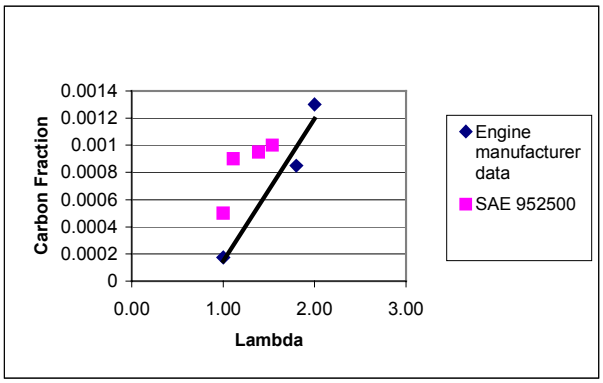

RESULTS

Figure 11 and 12 compare experimental data for a test cell operated engine with the combined catalyst and combustions models, showing predicted and actual conversion efficiencies for propane and NMHC respectively.

Figure 14 shows test data for CO, NOx, propane and total diesel hydrocarbons, showing a good correlation for a variety of gas species, substrate types and operating conditions. Data was collected for both metal and ceramic substrates, a variety of cell densities, substrate geometries, engine types and operating conditions. In order to ensure operating conditions are fully controlled by the mass transfer regime, data points were collected on new or degreened catalysts, with inlet gas temperature > 500 ^{o}C for propane and > 400 ^{o}C for all other species. In addition, data for three-way catalysts was obtained only where the quality of air-fuel ratio control was very high. The results in Figure 14 demonstrate that for > 400 ^{o}C, a rich burn engine utilizing a high quality closed loop air-fuel ratio controller and catalyst, the rate limiting step for both CO and NOx is mass transfer controlled. The results also show that the correlation is very general and can be applied to different species, operating conditions, and catalyst types. The data corresponds well with literature [15, 16].

Table 4 – Test Conditions

Oxidation Catalyst Coating A
200 cpsi
metal substrate
SV = 109000 h-1
Cummins 5.9 G
Oxygen, Exhaust 3%

Figure 11 – Light-off curve for propane with non-first order reaction kinetics

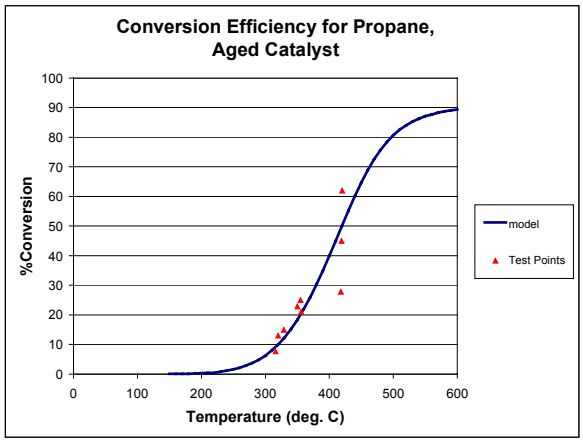

Figure 12 – Light-off curve for non-methane hydrocarbons, engine running on natural gas. Breakdown of NMHC speciation was determined by model.

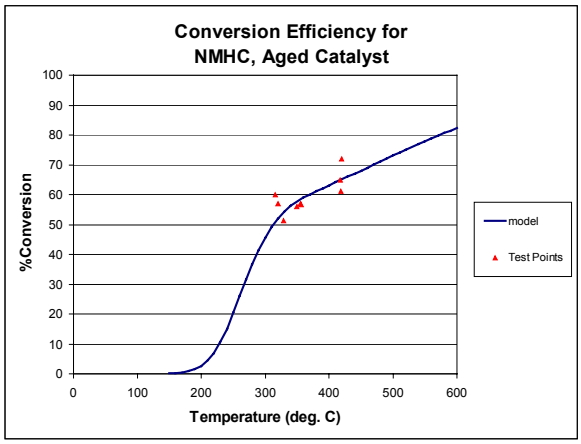

Figure 13 – Comparison of non-methane hydrocarbon composition (fuel vs. raw engine-out emissions), commercial quality gas Ontario, Canada 2003.

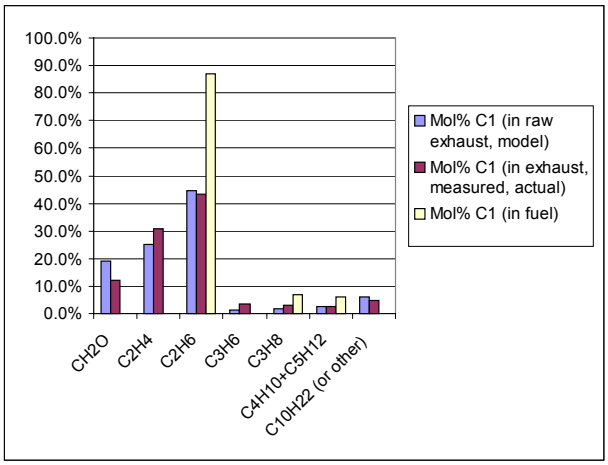

Figure 14 – General mass transfer correlation

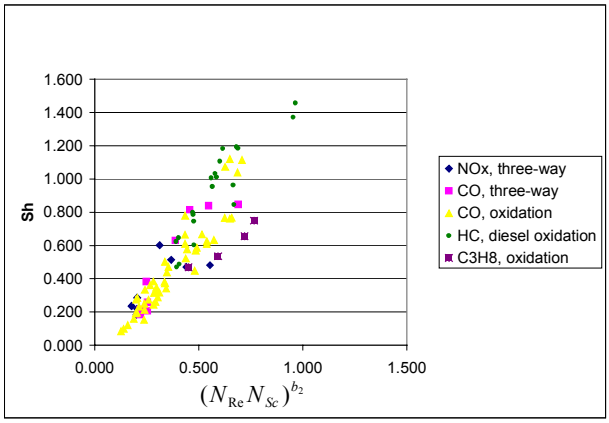

CONCLUSIONS

A predictive catalyst model used for stationary industrial engines is described. This model considers the differences in the catalyst types, substrate/washcoat properties, catalyst aging and fuel composition. The validity of the model is shown by example case studies, where results show excellent correlation between the model and test cell and field data for a wide range of engines, catalyst types and operating conditions. It is also shown that a mass transfer correlation is determined that is applicable for a variety of different pollutant species, catalyst geometries, cell density, and it can be used for three-way and oxidation catalysts.

NOMENCLATURE

a Geometric surface area of washcoated substrate per unit volume of substrate (m^2/m^3)

A Frequency factor (1/s)

A_c Cross-sectional area (m^2)

b_1, b_2 Experimentally determined constants for mass transfer correlation (-)

C_{As} Concentration of gas phase species A at the surface of washcoat (mol/m^3)

C_A Concentration of species A in bulk gas of channel (mol/m^3)

$C_{g,i}$ Gas concentration (mol fraction) of species i

c_{pgm} Empirical value correlated to platinum/paladium/rhodium loading of washcoat (arbitrary dimensions)

c_{pg} Specific heat at constant pressure of gas (J/kg/K)

c_{ps} Specific heat of solid (J/kg/K)

d Channel diameter (m)

D_{AB} Diffusivity of species A in bulk gas B (m^2/s)

E_A Activation energy (J/mol)

F_{in} Molar rate in, (mol/s)

F_{out} Molar rate out, (mol/s)

h Heat transfer coefficient ($J/m^2/s/K$)

$-\Delta H$ Heat of reaction (J/mol)

k_c Mass transfer rate term (m/s)

k_c^i Intrinsic mass transfer rate term (s^{-1})

k_r Kinetic reaction rate term (m/s)

k_r^i Intrinsic kinetic reaction rate term (for first order reaction, s^{-1})

$K_{overall}$ Overall reaction rate term (m/s)

L Length of substrate (m)

$\dot{m}_g$ Exhaust mass flow (g/s)

M_g Molecular weight of exhaust (g/mol)

N_{Re} Modified Reynolds number, $N_{\mathrm{Re}} = \frac{\rho_g V}{\mu a}$

N_{Sh} Sherwood number, $N_{Sh} = \frac{k_c}{D_{AB} a}$

N_{Sc} Schmidt number, $N_{Sc} = \frac{\nu}{D_{AB}}$

r Rate of reaction (mol/m^2-s)

R Radius of substrate (m), universal ideal gas constant (J/mol-K)

Re Reynolds number, $\mathrm{Re} = \frac{\rho_g V d}{\mu}$

S_{BET} BET Surface area of washcoat (m^2/g)

t Time (s)

T Temperature (K)

T_g Gas temperature (K)

T_s Substrate/washcoat temperature (K)

V Interstitial (in-channel) gas velocity (m/s)

v Superficial gas velocity (m/s)

X Fraction of species converted (-)

z Axial distance (m)

Greek symbols

ε Void volume fraction (-)

ρ_g Gas density (g/m^3)

ρ_s Solid (substrate) density (g/m^3)

ρ_{wc} Density of washcoat (g/m^3)

λ_s Thermal conductivity of solid (W/mK)

ν Kinematic viscosity (m^2/s)

η Effectiveness factor of washcoat (-)

γ Flow uniformity index

μ Dynamic viscosity of gas (g/m-s)

ϖ Emipirical exponential value correlated to Platinum Group Metal loading of washcoat (-)

REFERENCES

[1] Wanker, R., et. al., New physical and chemical models for the CFD simulation of exhaust gas lines: A generic approach, SAE 2002-01-0066.

[2] Konstantinidis, P., Computer-Aided Design and Optimization of Catalytic SI Engine Exhaust After-Treatment, Ph. D. Thesis, Aristotle University, Thessaloniki (1997).

[3] Siemund, S., D. Schweich, J.P. Leclerc, J. Villermaux, Modelling Three-Way Monolithic Catalytic Cenverter: Comparison Between Simulation and Experimental Data, in "Catalysis and Automotive Pollution Control III, ed. A. Frennet and J.M. Bastin, Elsevier Science B.V., (1995).

[4] Leclerc, J.P., D. Schweich, Modeling Catalytic Monoliths for Automobile Emission Control, in "Chemical Reactor Technology for Environmentally Safe Reactors and Products", ed. H.I. de Lasa, G. Dogu and A. Ravella, Kluwer Academic Publishers (1992), p. 547-576.

[5] Fogler, H.S., Elements of Chemical Reaction Engineering, Prentice-Hall (1986).

[6] Froment, G.F., K. B. Bischoff, Chemical Reactor Analysis and Design, 2nd ed., John Wiley & Sons, Inc. (1990).

[7] D. Schweich, Laboratory Data for Three-Way Catalytic Converter Modelling, in "Catalysis and Automotive Pollution Control III, ed. A. Frennet and J.M. Bastin, Elsevier Science B.V., (1995).

[8] Leprince, T., J. Aleixo, K. Chowdhury, M. Naseri, S. Williams, Development of Pre-Turbo Catalysts for Natural Gas Engines, ASME ICE2003-568.

[9] Oh, Se. H.; Cavendish, J.C., Transients of Monolithic Catalytic Converters: Response to Step Changes in Feedstream Temperature as Related to Controlling Automobile Emissions, Ind. Eng. Chem. Prod. Res. Dev., 21, 29-37 (1982).

[10] Idelchik, I.E., Handbook of hydraulic resistance, 3rd ed., CRC Press, Inc., (1994).

[11] Exhaust Flow Performance and Pressure Drop of Exhaust Components and Systems, SAE Course Notes, (2002).

[12] Pattas, K.N. et. al., Computer Aided Assessment of Catalyst Ageing Cycles, SAE 950934.

[13] Poulsen, J.H., J.S. Wallace, Operating Parameter Effects on the Speciated Hydrocarbon Emissions from a Natural Gas Fueled Engine, SAE 942007.

[14] Crawford, J.C., J.S. Wallace, Engine Operating Parameter Effects on the Speciated Aldehyde and Ketone Emissions from a Natural Gas Fueled Engine, SAE 952500.

[15] Vortuba et. al., Heat and Mass Transfer in Honeycomb Catalysts-II, in Chemical Engineering Science, Vol. 30, pp. 201-206, (1975).

[16] Ullah, U., et. al., Monolithic Reactors: Mass Transfer Measurements Under Reacting Conditions., Chemical Engineering Science, Vol. 47, no. 9-11, pp. 2413-2418, (1992).

[17] Gassman, I., Combustion, 2nd Ed., Academic Press, Inc., (1987).